AIAA JOURNAL
Vol. 46, No. 4, April 2008

Leading-Edge Separation Control by Means of Pulsed Vortex Generator Jets

Peter Scholz,* Marcus Casper,† Jens Ortmanns,‡ Christian J. Kähler,§ and Rolf Radespiel¶
Technical University of Brunswick, 38106 Braunschweig, Germany

DOI: 10.2514/1.26176

An airfoil was designed to stall with an abrupt turbulent leading-edge separation and equipped with a pneumatic system for active flow control. The system pulses compressed air through 45 deg skewed slots. Depending on the position of the slots, two very different behaviors were found. With the actuators positioned in the region of the separation line, the control system could not prevent separation. However, a very advantageous influence on the separation resulted with even higher normal forces than in prestall condition. The duty cycle was found to be the major control parameter for this kind of control. When the actuation was positioned well in front of the separation line the influence of the actuation system on the stall behavior changed completely. Here the system was able to prevent the leading-edge separation. The influence of the duty cycle becomes much weaker and maximum normal force scaled mainly with the mean ejected momentum, varied either by the duty cycle or the supply pressure.

Nomenclature

A_{sl}	=	total slot exit area
A_W	=	wing area
c	=	chord length
c_{np}	=	normal force coefficient
c_w	=	drag coefficient
c_μ	=	momentum coefficient
F^+	=	reduced frequency, $f \cdot c/u_\infty$
f	=	excitation frequency
H_K	=	boundary-layer shape factor
l	=	length of actuator slot
p_V	=	supply pressure
Re	=	Reynolds number
u, v, w	=	velocities
u_e	=	boundary-layer edge velocity
u_j	=	jet exit velocity (mean exit velocity during active phase)
u_∞	=	freestream velocity
$\dot{V}_j$	=	flow rate in pressure supply system
x	=	chordwise coordinate
y	=	spanwise coordinate
z	=	remaining coordinate
α	=	angle of attack
Δ	=	duty cycle
Θ	=	boundary-layer momentum thickness
Λ	=	aspect ratio of actuator slot
λ_e	=	local velocity ratio based on u_e, $\lambda_e = u_j/u_e$

Presented as Paper 2850 at the 3rd AIAA Flow Control Conference, San Francisco, California, 5–8 June 2006; received 26 June 2006; revision received 6 December 2007; accepted for publication 9 December 2007.

*Research Scientist and Ph.D. Candidate, Institute of Fluid Mechanics, Bienroder Weg 3; p.scholz@tu-bs.de. Member AIAA.

†Research Scientist and Ph.D. Candidate, Institute of Fluid Mechanics; m.casper@tu-bs.de.

‡Research Scientist and Ph.D. Candidate, Institute of Fluid Mechanics; j.ortmanns@tu-bs.de. Member AIAA.

§Head of Work Group "Flow Control and Measuring Techniques," Institute of Fluid Mechanics; c.kaehler@tu-bs.de.

¶Professor, Institute of Fluid Mechanics; r.radespiel@tu-bs.de. Senior Member AIAA.

I. Introduction

ACTIVE control of flow separation is gaining importance in research and industrial applications. In the past, it was shown by several researchers that a separating boundary layer can be stabilized by static or dynamic jets. Such actuators can be used in several different scenarios.

A tangential injection of compressed air is quite evident. The intention is to add momentum directly to the lower regions of a separating boundary layer. This method is known for a long time [1], but tangential blowing becomes more and more ineffective as the surrounding velocity becomes higher. Therefore, this kind of actuation is not very efficient for leading-edge separation control, because the high velocities in the suction peak of an airfoil would require huge flow rates at full-scale Reynolds numbers. Tangential blowing might be applied to low speed regimes of an airfoil, especially if large flow rates can be accepted and if secondary effects, such as the Coanda effect, can be used [2].

The efficiency of tangential blowing can be excessively raised by using a dynamic (periodic) jet rather than a static one [3]. The pulsing introduces periodic vortical structures, which increase the turbulent mixing between the low momentum fluid close to the surface and the outer parts of the boundary layer. This allows the mean (net) mass flux to be reduced, because the momentum is taken from the outer flow and not from the actuator jet itself, which only catalyzes the transfer. This oscillatory blowing has been successfully applied to airfoils even under flight conditions [4]. The efficiency is remarkable, as the net mass flux can be reduced to zero by alternating blowing and suction. The excitation frequency f is chosen to be in the order of magnitude of a surrounding, naturally unstable frequency [5], the shedding frequency of the shear layer f_{sl}, for example. The vortices of the shear layer are stimulated by the actuator, resulting in an amplification mechanism. In the following, this kind of flow control will be referred to as "2-D control," because the actuation system is usually not altered in the spanwise direction (probably beside some fabrication limits, like small stiffeners to retain the structural integrity of the slot). Because the dominant effect is the introduction of periodicity, the device itself is not of primary importance. 2-D actuation techniques are published with tangential blowing, vibrating flaperons [3,6], piezoelectric actuators [7], or wall-normal spanwise slots [8], for example.

The latter should be mentioned, because it was found to be very efficient on the fowler flap of a high-lift configuration [9] in which the shear layer formed by the wake of the main element and the jet through the flap gap sheds distinct and strong wake vortices that can be stimulated very well.

The introduction of streamwise vortices is also well known as a means for delaying flow separation [10,11]. Again, the beneficial effect is the enhanced mixing of the boundary layer. Streamwise

vortices are classically introduced by mechanical vortex generators [10,12], but can also be generated by pitched and/or skewed circular jets [13–15] or by blowing through pitched and/or skewed slots [16,17]. Actuators that intend to introduce streamwise vortices are usually called "vortex generator jets." In the following, the control principle will be referred to as "3-D control," because unlike the case of 2-D control a local 3-D structure is used. The mass flux can become significant for the vortex generator jets as the effectiveness scales with the exit velocity u_j or the local velocity ratio λ_e. First, the pulsing was introduced to save mass flux over a certain part of the period, but it could be shown that pulsed actuators are more effective than steady ones [13,18]. The reason for this is associated with the impulsively started jet flow, which strengthens the primary vortex. Furthermore, due to the inactive parts during dynamical actuation the streamwise vortices descend deeper into the boundary layer and reside closer to the wall [19]. Probably a link between 2-D control and unsteady 3-D control may be found. As a matter of fact, it is not yet clearly known if the two principles can be combined, for example, if a *dynamic* vortex generator jet (that is usually designed to create strong streamwise vortices) will generate spanwise vorticity, which is strong enough to encourage some stimulation effects. Fasel et al. [20] described this "combination effect," however, in a scenario in which laminar separation had to be prevented.

Apart from the aforementioned classification into 2-D or 3-D control strategies, the active control of flow separation can be divided into two boundary condition categories. All of the aforementioned systems concentrate on nonseparated or partially separated flows, which using the definition of Wu et al. [21] can be referred to as "separation control" or, more precisely, as "separation delay." The second category is usually called "poststall flow control" or "control of separated flow," as it deals with already separated flows such as airfoils at very high angles of attack (AOA) or bluff bodies, which can be influenced advantageously by using enhanced vortex shedding or by stimulating shear layers. In terms of actuator technology, poststall flow control is closely related to 2-D separation control; the flow is actuated by, for example, synthetic jets or leading-edge flaps (see Wu et al. [21] and references therein).

Future aircraft need to be lighter, quieter, and less complex. It is therefore interesting to reduce the number of elements of the high-lift configuration. A flapless wing is not realistic, because the flap carries an important amount of the lift. The slat, on the other hand, does not contribute a great amount to lift but rather is a kind of passive flow control, as it prevents separation on the main element and allows for greater angles of attack [22]. A convenient way to reduce the system's intricacy is to replace the slat with a device that is significantly less complex.

Two-element (slatless) airfoils at high angles of attack develop pronounced leading-edge suction peaks, resulting in strong adverse pressure gradients. It is likely that the turbulent boundary layer does not separate at the trailing edge (the "common" scenario), but at the leading edge, which results in a very abrupt loss of lift. This "turbulent leading-edge stall" is the scenario that the proposed active flow control device has to face. (The term leading-edge stall often refers to a low-Reynolds-number stall phenomenon, in which a small-scale laminar separation bubble bursts. This bubble burst is unlikely with reasonably high Reynolds numbers and is *not* the kind of stall that is important for full-scale transport aircraft.)

II. Airfoil Design

To test the actuator setup and integration in a realistic environment, a proper airfoil was designed and built. In a relatively small wind tunnel, highly cambered multi-element configurations cannot be tested well, because the necessary corrections for wake blockage and streamline curvature can become a significant part of the effectively measured coefficients [23]; preliminary calculations of a two-element airfoil showed a necessary correction of c_l of as much as 20%. Because of this fundamental problem, it was decided to design a moderately cambered one-element airfoil.

However, the aim is to test the actuators in an environment that is as close to an in-flight scenario as possible. The Reynolds number is limited to $Re = 1.3 \times 10^6$. Nevertheless, the pressure distribution, the boundary-layer development, and the stall behavior should be similar to that of a two-element high-lift airfoil close to stall. The reference two-element airfoil was derived from a state-of-the-art three-element configuration by retracting the slat. The properties and the boundary-layer development were then analyzed with the Euler code MSES, and the one-element airfoil was designed with the panel code XFOIL to have a similar boundary-layer development. Both the MSES and XFOIL codes have been developed by Drela et al. [24,25]; they have the same boundary-layer code integrated and are widely accepted in the airfoil design community. It is known that the results of the boundary-layer codes agree very well with measurements, as long as turbulent separation is not an issue. The reference case was therefore chosen to be at an AOA of the two-element airfoil of $\alpha = 8.0$ deg, which is close to but not yet stalled.

The major difference in the upper side pressure distributions of two- and one-element configurations is the fact that, for the two-element airfoil, the flow at the trailing edge of the main element does not decelerate to u_∞. Hence, the trailing edge c_p is negative. It is therefore not possible to copy the pressure distribution to a one-element airfoil. However, the boundary-layer development results from a certain pressure-gradient distribution rather than from local c_p. A one-element version can therefore be derived by starting at the trailing edge ($c_p \approx 0.1$) and then running backward along the upper side with the desired pressure gradient, which results in a certain upper side pressure distribution that in turn can be transferred into an airfoil contour. Because c_p at the trailing edge is greater for the one-element airfoil, this procedure results in a greater $c_{p,\min}$ in the suction peak, but the local pressure gradients are essentially copied and therefore the boundary layer develops in a very similar way.

Figure 1a displays a comparison of the pressure distributions c_p for the reference two-element airfoil with the one-element design. As the one-element airfoil has a strongly reduced camber, the zero-lift AOA does not correspond. Therefore, the two-element airfoil is shown at $\alpha = 8.0$ deg and the one-element airfoil at $\alpha = 13.7$ deg. For a better comparison, the pressure distribution of the one-element airfoil is shown along with one that was displaced by adding a constant Δc_p. It can be seen that the displaced distribution agrees very well with the reference distribution. In these cases, the airfoils were analyzed with free transition. Therefore, a little bump due to transition over a laminar separation bubble appears; the size as well as the position of this bubble is represented correctly by the one-element design. Note that the free-transition computations are shown to demonstrate how similarly the boundary layer develops, whereas the measurements presented here were made with a fixed transition. Figure 1b displays the corresponding upper side pressure-gradient distribution on a negative, logarithmic scale. A good similarity can be maintained along the airfoil chord length. From $x/c = 0.5$ toward the trailing edge, some deviations are visible where the pressure distribution of the design had to be adjusted to fit the trailing-edge pressure and to circumvent trailing-edge stall.

A comparison of the main boundary-layer parameters is given in Fig. 2. Naturally, for both the two-element airfoil and the one-element design, the stagnation pressure is $c_p = 1.0$. Because the two-element airfoil has a lower $c_{p,\min}$, the flow upstream of the suction peak is accelerated more, which can neither be circumvented nor balanced. This difference results in slightly different boundary layers. All parameters agree quite well for the first 20% of the airfoil chord but further downstream the agreement vanishes gradually, which is a result of the longer-lasting acceleration and the higher edge velocity of the reference airfoil. Anyway, for stall and actuation, the leading-edge area is of primary interest and a certain aberration toward the trailing edge is acceptable.

The designed airfoil, PS03-8.27, is schematically shown with its equipment in Fig. 3.

III. Experimental Setup

For the experiments, a wind-tunnel model with a wingspan of 1.3 m and a chord length of $c = 400$ mm was built. The actuators

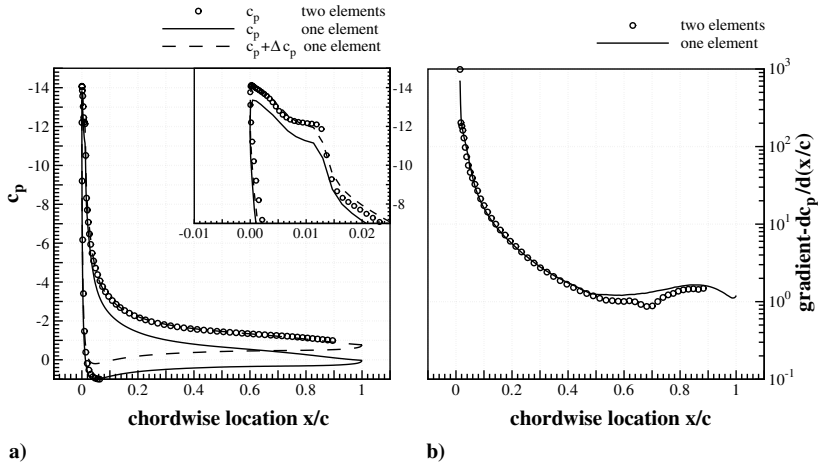

Fig. 1 Comparison of the two-element reference airfoil and the one-element design (reference, $\alpha = 8.0$ deg; design, $\alpha = 13.7$ deg; both airfoils, $Re = 1.3 \times 10^6$): a) pressure distributions, and b) pressure gradients.

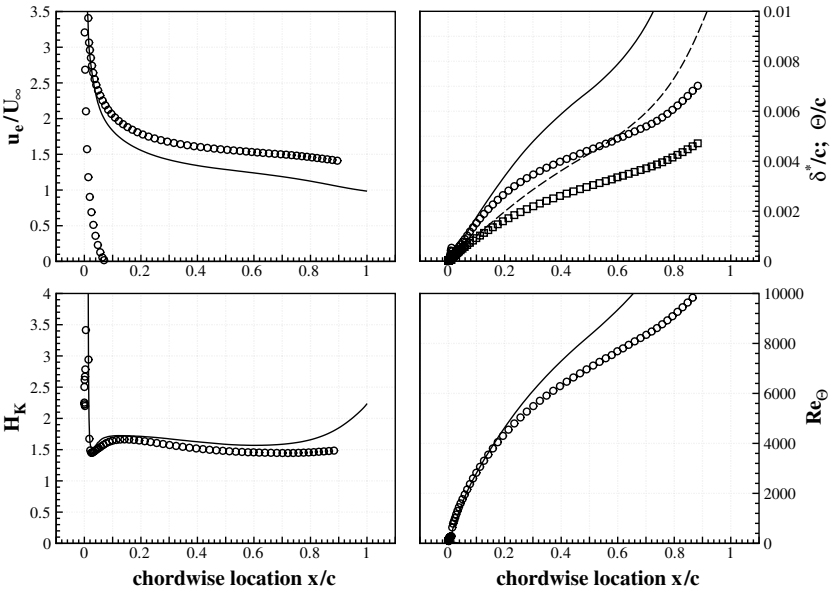

Fig. 2 Boundary layer data: edge velocity u_e/U_∞, displacement thickness δ^*, momentum thickness Θ, shape factor H_K, and Reynolds number based on the momentum thickness Re_Θ of the two-element reference (denoted by symbols) at $\alpha = 8.0$ deg compared with the one-element design (denoted by lines) at $\alpha = 13.7$ deg.

have to be integrated in the nose region of the airfoil to prevent the collapse of the suction peak at high AOA, therefore the nose is milled numerically controlled from a solid aluminum block to allow the integration of settling chambers. It is fitted to a carbon-fiber body with a bolted joint. According to preliminary studies, the airfoil is equipped with the following actuator system (see Fig. 3): compressed air is piped through the pressure supply line into 20 electromechanical fast-switching valves, which are controlled by a multichannel frequency generator that can generate arbitrary duty cycles. The duty cycle Δ is defined as the portion of the period in which the valve is open, for example, $\Delta = 25\%$ at 100 Hz means the valve opens, closes after 2.5 ms, and remains closed for 7.5 ms. Static actuation means the valves are constantly open and the actuators function like steady vortex generator jets.

The valves are commercial units (Festo's type MH2) that can run with reasonably high frequencies ($f_{\max} \approx 150$ Hz without leakage flows) and adequate feeding pressures ($p_{V,\max} \approx 8.0$ bar). They can only adopt "open" and "closed" positions; sinusoidal or any kind of nonsquare actuation is not possible. The exits of the valves are connected with the settling chambers; each valve feeds one individual 60-mm-wide settling chamber. A groove is milled into the aluminum on top of the settling chambers, and small plastic inserts are glued into these grooves to close the chambers. The inserts were fabricated by stereolithography to allow the integration of the slots; after gluing them to the aluminum, they were ground in to fit flush with the airfoil's surface.

The actuator optimization procedure cannot be outlined here. Different ones were studied in detail by means of flat plate experiments concerning their dynamical behavior [26], the generation and decay of the streamwise vortices [19], their optimal orientation, and the optimal distance and setup for a spanwise array of actuator slots [27]. A comprehensive overview is given elsewhere [28]. According to these studies, skewed slots with a skew angle of 45 deg were chosen. The length was $l/c = 0.125$ with a slot aspect ratio of $\Lambda = 25$. The jets emerge normal to the airfoil's surface; individual slots were staggered alternately with a spacing of $\Delta y = 3 \cdot l \hat{=} \Delta y/c = 0.0375$. The airfoil has a total of 80 individual slots. The CAD close up in Fig. 3 highlights the arrangement of the slots; Fig. 4 displays the airfoil with the internals. One uncertainty concerning the transfer from the flat plate experiments for optimization to the airfoil was the scaling. Based on momentum thickness Θ, the actuator slots at the airfoil are 2 times larger, $l/\Theta \approx 18$ at the airfoil compared with $l/\Theta \approx 10$ at the flat plate, whereas $Re_\Theta = 1550$ applies for both (based on the measured

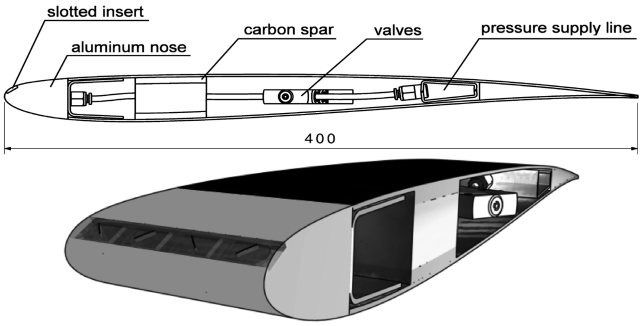

Fig. 3 Schematic drawing of the airfoil PS03-8.27 with the actuation setup and CAD close up of the nose, showing the aluminum assembly and the insert with the alternately oriented slots (5×0.2) mm^2, $\beta = \pm 45$ deg, and $\Delta y = 3 \cdot l$.

Fig. 4 Highly equipped airfoil, shown here with removed covers on the bottom side to highlight the actuation setup.

momentum thickness for the flat plate and the XFOIL-calculated momentum thickness at the position of separation $x/c = 0.05$ for the airfoil at $c_{np} = 1.2$, $Re = 1.3 \times 10^6$). The larger size was necessary because smaller slots cannot be fabricated well enough.

The amplitude of the pulsation was controlled by a pressure reducer, which was installed outside the model and controlled the supply pressure p_V. The flow rate $\dot{V}_j$ was measured using a pressure compensated variable area flow meter. The momentum coefficient c_μ is defined as

$$c_\mu = \frac{\rho_\infty \cdot \dot{V}_j \cdot \Delta \cdot u_j}{\frac{\rho_\infty}{2} \cdot u_\infty^2 \cdot A_W} \tag{1}$$

The jet exit velocity is related to the flow rate

$$\rho_\infty \cdot \dot{V}_j = \rho_j \cdot \Delta \cdot u_j \cdot A_{\mathrm{sl}} \tag{2}$$

and therefore

$$c_\mu = \frac{2 \cdot \dot{V}_j^{\,2}}{u_\infty^2 \cdot A_{\mathrm{sl}} \cdot A_W} \cdot \frac{\rho_\infty}{\rho_j} \tag{3}$$

Table 1 Jet exit velocity, momentum coefficient, and percentage of compressibility correction for $\Delta = 50\%$

p_V, bar	u_j, m/s	c_μ, %	Corr., %
1.0	98	0.03	2.6
2.0	206	0.14	8.5
3.0	275	0.26	15.5
4.0	331	0.41	23.4

Neither the jet exit velocity u_j nor the jet exit density ρ_j can be determined by direct measurement, although the high exit velocities cause compressibility effects that make it unfeasible to assume ρ_∞ in the jet. With a first assumption $u_j \approx \dot{V}_j/(\Delta \cdot A_{\mathrm{sl}})$ an iterative solution algorithm based on an isentropic model was started to correct the jet density. The outcome is a corrected exit velocity u_j and a corrected c_μ, respectively. Table 1 gives an exemplary overview for $\Delta = 50\%$. It should be noted that the flow is evidently not isentropic, therefore the correction is not exact. It was checked that the valves are accurate enough so that Table 1 does not depend on the frequency. In the preliminary studies of the actuation system, no noteworthy appearance of cavity resonances or ringing was found [26].

The flow meter is accurate to approximately 5% ($\sigma \dot{V}_j = 10\,l/\mathrm{min}$); the pressure can be set with an accuracy of 2% ($\sigma p_V = 0.1$ bar), resulting in an overall (measurement) accuracy for c_μ of 10%. It is known for jet vortex generator jets that efficiency is associated with jet exit velocity u_j (or local velocity ratio; refer to Introduction) which in turn is roughly proportional to the supply pressure. Therefore, parameter variations were usually made with constant supply pressure p_V.

It was found in ZPG flat plate experiments that an area of retarded (blocked) flow is present right behind the exit slots [27], which vanishes approximately $x/l = 2 \sim 3$ behind the orifice and is followed by a long area of efficient momentum transport. Because the slots at the airfoil have a length of $l = 5.0$ mm, it is expected that their region of efficient momentum transport starts approximately $x = 15$ mm downstream, which in turn equals $x/c = 3.75\%$. URANS computations predicted the initial separation at $x/c \approx 5\%$; the centers of the orifices were therefore initially located at $x/c = 1\%$.

The experiments were performed in the 1.3 m $\times$ 1.3 m closed loop atmospheric tunnel ($Tu = 0.2\%$ at 40 m/s) located at the Technical University of Brunswick.** The freestream velocity was constantly set to $V = 50$ m/s, giving a Reynolds number of $Re = 1.3 \times 10^6$. The airfoil has 31 static ports; for both setups, these ports were located between a "common-flow-up" configuration. The facility is equipped with a wake rake behind the airfoil to capture the total and the static pressure in the wake. All pressure ports were connected to a PSI 8400 SDI multichannel pressure transducer with an accuracy of better than 0.12%. The normal force coefficient c_{np} was determined by integrating c_p along x/c, and drag c_d by integrating the wake pressures following Jones's approach [29]. Wake rakes cannot measure drag in largely separated states [23]. The lift coefficient c_l, on the other hand, cannot be determined from the pressure distribution if the drag is unknown. Therefore, the normal force coefficient c_{np} will be used throughout the paper for better comparability. The data were not corrected for tunnel-wall interferences. The analysis focuses on the relative change between configurations, which is not significantly influenced by tunnel-wall interferences.

The particle image velocimetry (PIV) measurements were made with a standard setup consisting of a LaVision Imager pro X 11 megapixel camera with either an Infinity K2 long-distance microscope or a telephoto lens with a 360 mm focal length. The flowfield was illuminated with two Brilliant Nd:YAG lasers with 160 mJ per pulse. The spatial resolution of the final vector fields is

**Data available online at http://www.tu-braunschweig.de/ism/institut/wkanlagen .

0.5 mm. The accuracy of the measurements is nominally 0.05 pixels [30] or $\sigma u \approx 0.875$ m/s. To avoid surface reflections, the aluminum nose was polished. All presented vector fields are a temporal mean value of 250 individual recordings.

As mentioned previously, the term leading-edge stall usually refers to a burst of a laminar separation bubble, which is not supposed to occur on this airfoil. Nevertheless, the relatively low Reynolds number of $Re = 1.3 \times 10^6$ is typical for such problems and, indeed, the free-transition case shows a separation bubble that has to be avoided by using a proper transition tripping; here, a 50-μm-thick and 2-mm-wide sticky tape was placed at $x/c = 0.3\%$.

IV. Results I: Airfoil with Suction-Side Actuation

Turbulent leading-edge stalls are challenging to measure because large regions of separated flow appear suddenly. This typically leads to stall cells, which are associated with highly three-dimensional patterns called "owl eyes" [31]. Under such conditions, the location of the pressure ports might not give a representative picture of the overall flow state, and the measurements are consequently questionable concerning the validity of c_{np}. During all measurements, tufts were attached to the model to monitor the flow state and to decide if the pressure distribution is valid and representative. The presented clean case is one in which separation starts at $\alpha \approx 10.5$ deg at the intersection of the model with the wind-tunnel wall. The separated area then grows in size and finally, at $\alpha \approx 14.5$ deg, one big stall cell appears in the center of the airfoil; the development of this central stall cell is associated with a sudden loss of lift. This case was found to give the most representative data at the pressure ports.

Additionally, extensive tuft visualizations were carried out to analyze the stall behavior with actuation. As a matter of fact, these visualizations highlight that, as soon as pulsed blowing is introduced, the owl eyes disappear and all tufts move irregularly. Test were made with stalling the airfoil and then initiating the forcing, turning on the flow control system and then sweeping the airfoil into stall, and additionally with AOA backward and forward sweeps. All of the methods led to the same pressure distributions. The airfoil flow with pulsed blowing is very repeatable and free of hysteresis. This advantageous behavior was mentioned by many others, for example, Hites et al. [32].

In Fig. 5a, the c_{np} curves for the clean cases with free and fixed transition are shown. As expected, the airfoil with fixed transition stalls at a much higher AOA because the bubble burst is prevented. The fixed transition case still reveals a small hysteresis loop. However, this is a result of the stall cell structures and not an effect of a separation bubble.

A variation of the duty cycle is given in Fig. 5b for the case $F^+ = 0.6$ and $p_V = 1.5$ bar. The duty cycle has great influence on the efficiency of the stall control system. For $\alpha < 14.5$ deg, the small duty cycles provide higher c_{np} whereas the larger duty cycles have an unfavorable effect. Around $\alpha = 14.5$ deg, all of the curves show some kind of a "kink," but whereas for the clean case this is associated with a deep stall, the normal force of the controlled cases rises again. For a duty cycle of $\Delta = 12\%$, the maximum c_{np} can be achieved at $\alpha = 16$ deg. For higher AOA, the slightly higher duty cycles are more effective; $\Delta = 25\%$ reaches its maximum at $\alpha = 19$ deg. Greater duty cycles (or more general greater c_μ) do not provide further advantage and neither does static actuation.

The influence of the frequency on normal force c_{np} and drag c_d is shown in Fig. 6 for a duty cycle of $\Delta = 25\%$ and an amplitude of $p_V = 1.5$ bar. In a prestall condition $\alpha < 14.5$ deg, the frequency does not have any influence, because there is no potential for flow improvement. The control rather has a disadvantageous influence on the normal force as well as on the drag. At $\alpha \approx 13.5$ deg, the lift curve shows the kink and the drag rises, which allows the assumption that the airfoil stalls. As soon as this has happened, c_{np} of the controlled airfoil rises. The frequency now has an influence, though it is not as vital as the influence of the duty cycle. The drag coefficient rises in any case. Although the flow control system can increase the normal force and shift $\alpha_{\max}$ to higher values, the drag rise due to separation is not significantly influenced.

Figure 7 (refer back to Fig. 5b for the c_{np} curves) displays three pressure distributions at $\alpha = 19$ deg. Note that the short duty cycle $\Delta = 25\%$ compared with the static actuation increases c_p in the suction peak, but lowers c_p near the midchord. Figure 8 depicts corresponding PIV measurements across the nose section. The measured plane is located $\Delta y/c = 0.2388$ from the central section of the airfoil, across the symmetry axis of two common-flow-up slots. Additional measurements were made across one slot and across the symmetry axis of two "common-flow-down" slots to ascertain that the spanwise location does not have an effect; as a matter of fact, the longitudinal vortices themselves are too small to be resolved in this setup.

The clean case is completely separated. However, the turbulent kinetic energy of the shear layer is quite low, showing that the shear layer is mostly steady. When actuation is turned on with a duty cycle of $\Delta = 25\%$, the flowfield changes in three ways. The separation starts slightly further downstream, therefore the shear layer is closer to the airfoil's contour and the turbulent kinetic energy level is substantially higher. But anyway, the separation has not been prevented. The PIV measurements were not triggered to the actuation process, and so the displayed flowfield is not phase locked but the high kinetic energy is not a simple result of averaging the unsteadiness of the actuation process. This can be concluded when comparing the $\Delta = 25\%$ case (Fig. 8b) to the static actuation case (Fig. 8c). Although the actuation is static, the turbulent kinetic energy level is high. Additionally, the shear layer is closer to the airfoil, and the separation starts even further downstream than in the case of

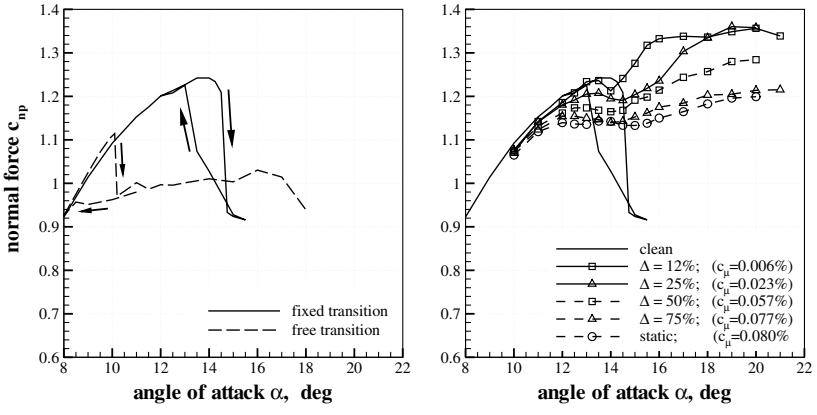

a) b)

Fig. 5 Normal force coefficients c_{np} over AOA α: a) clean cases, and b) variation of duty cycle Δ with $F^+ = 0.6$ and $p_V = 1.5$ bar.

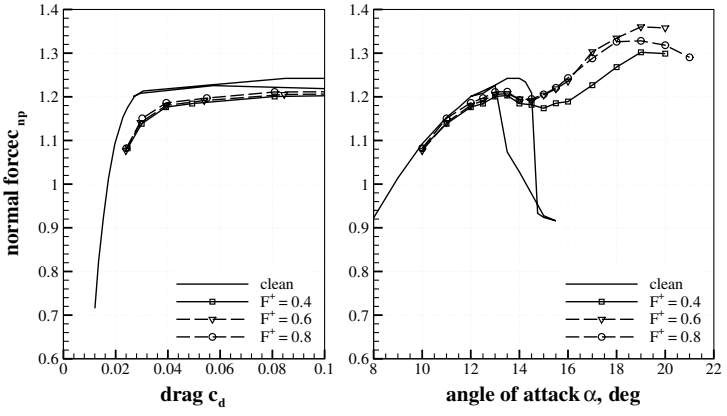

Fig. 6 Variation of frequency F^+ with $\Delta = 25\%$ and $p_V = 1.5$ bar; $c_\mu = 0.023\%$ for all cases: a) drag coefficient, and b) normal force coefficient over AOA.

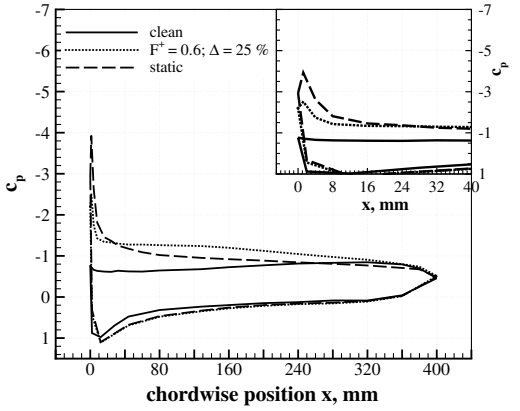

Fig. 7 Pressure distribution at $\alpha = 19.0$ deg, actuation with $p_V = 1.5$ bar.

unsteady actuation. This is consistent with the pressure distribution, for which the static case yields the smallest $c_{p,\min}$. Nevertheless, the $\Delta = 25\%$ case results in a higher c_{np} because of the lower c_p in the midchord section.

Although the actuation influenced the separation in a positive manner, it was not able to prevent it. Longer duty cycles or static actuation yields the lowest $c_{p,\min}$, whereas smaller duty cycles have an advantageous influence on the midchord pressure distribution. It is concluded that, for the given slot size, the position of the actuator orifices at $x/c = 1.0\%$ is too close to the initial point of separation. This gives an explanation for some of the effects that appear; close behind the slots there is an area of retarded flow. If this retarded flow is embedded into a boundary layer under a distinct adverse pressure gradient, a separation is provoked, which is an explanation for why c_{np} is decreased for smaller AOA. The kink in the c_{np} curve at $\alpha \approx 13.5$ deg is the transition from an attached into a separated flow state and is therefore associated with a rise of airfoil drag. But when the airfoil is separated, the actuators are not useless; they still introduce periodicity and consequently function as a poststall flow control device similar to those described by Wu et al. [21], Nishri and Wygnanski [6], and others. The smaller duty cycles reduce the amount of blockage and therefore increase efficiency while still introducing periodicity. Hence, the lower $c_{p,\min}$ in the midchord section is a result of the generation of spanwise vorticity and probably not due to longitudinal vortices.

To confirm or disprove this hypothesis, the next step was to vary the position of the actuators.

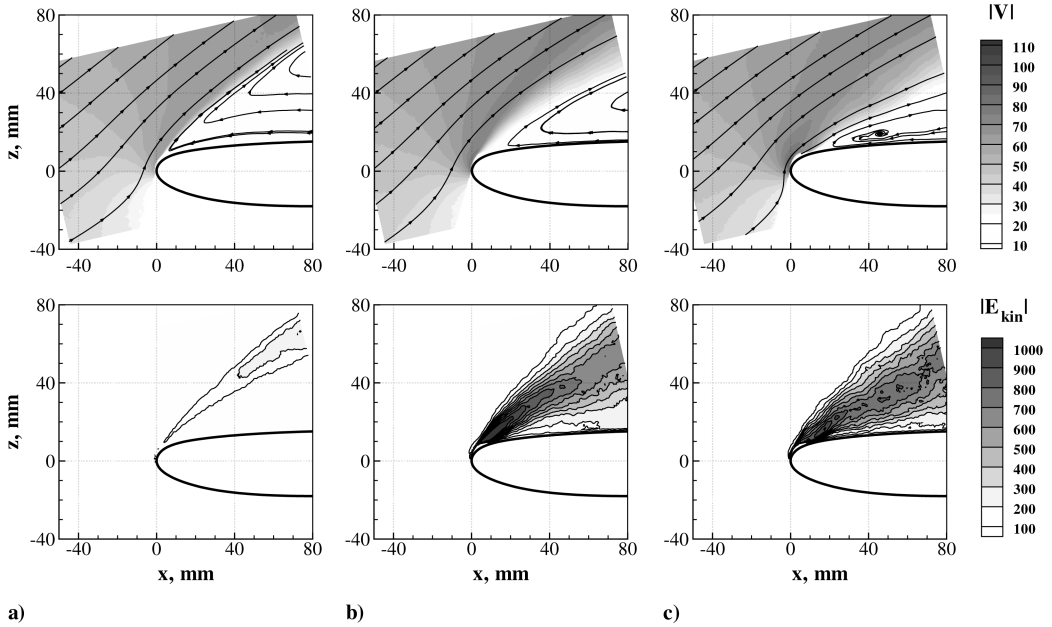

Fig. 8 Velocity magnitude $|V|$ (m/s), streamlines (upper row), and turbulent kinetic energy E_{kin} (m^2/s^2) for $\alpha = 19$ deg: a) clean case; b) $F^+ = 0.6$, $\Delta = 25\%$, and $p_V = 1.5$ bar ($c_\mu = 0.023\%$); and c) static blowing $p_V = 1.5$ bar ($c_\mu = 0.08\%$).

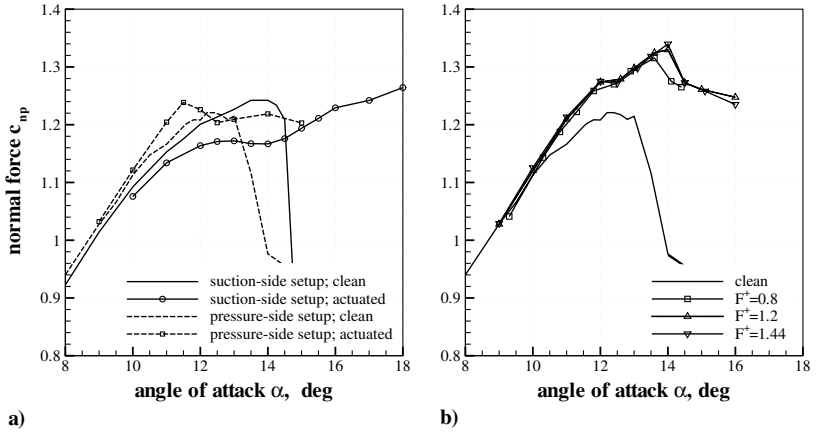

Fig. 9 Normal force coefficients c_{np} over AOA α: a) comparison of the reference and actuated cases for the pressure-side and suction-side setup, actuation $F^+ = 0.8$, $\Delta = 50\%$, and $c_\mu = 0.05\%$; and b) variation of frequency F^+ with $\Delta = 50\%$ and $p_V = 3.0$ bar, $c_\mu = 0.25\%$ for all cases.

V. Results II: Airfoil with Pressure-Side Actuation

By exchanging the aluminum nose, the position of the slots was moved to $x/c = 1.0\%$ on the pressure side. As the stagnation line is located further away from the leading edge, this pressure-side position is still upstream of the suction-side flow. To circumvent some of the limitations, the frequency generator and the pressure supply system were redesigned to allow for greater F^+ and greater c_μ.

The left side of Fig. 9 shows a comparison of the clean cases in the pressure-side and the suction-side setup. The maximum normal force as well as the maximum AOA slightly differ for the two different setups. This is not due to a different airfoil contour; the tufts showed a somewhat different behavior of the separated areas at the wind-tunnel wall intersections. However, unpublished experiences in other wind tunnels and with other models point out that the repeatability of low *Re* measurements dealing with turbulent leading-edge stalls is often relatively poor, and in this context the presented $\Delta\alpha_{\max} \approx 1.5$ deg is acceptable. The different maximum AOA might be an effect of the fact that the (always unsealed) slots are in a different location. Also included in Fig. 9a is a comparison of the suction-side actuation with the pressure-side actuation, both with $F^+ = 0.8$, $\Delta = 50\%$, and $c_\mu = 0.05\%$. It can clearly be seen that the different actuation principles behave very differently. Whereas the suction-side actuation lowers c_{np} for small AOA and reaches higher normal force in some kind of separated state at high AOA, the pressure-side actuation nearly linearly extends the c_{np} curve. This amplitude was the optimum one in the suction-side actuation setup, but in the pressure-side setup a further increase of c_μ revealed better effectiveness; Fig. 9b depicts the results of the pressure-side actuation and $c_\mu = 0.25\%$, which reaches much higher c_{np}. The curves shown are a variation of the reduced frequency. As a matter of fact, the influence of the frequency is weak so that the individual curves can hardly be differentiated. Higher frequencies seem to be a little bit more effective.

Figure 10 shows the drag and normal force for a variation of the duty cycle Δ with $F^+ = 1.44$ and $p_V = 3.0$ bar. Compared to the suction-side actuation (Fig. 6), the drag is raised less by the actuation. Furthermore, when the clean airfoil is not stalled the normal force is not decreased by the actuation system. The drag rise due to separation can be shifted to much higher normal forces with active control; note that the point of sudden drag rise is at $c_{np} \approx 1.15$ for the clean case. Using this as a criterion, the active control system shifted the onset of separation by $\Delta c_{np} \approx 0.2$. Concerning the operational parameters, the short duty cycle $\Delta = 25\%$ is less effective than the longer ones. However, when approaching $c_{np,\max}$ the dynamic actuation with $\Delta = 50\%$ is slightly more effective than the static one, although the static one needs much more momentum c_μ.

Figure 11 plots the maximum normal force for the different cases over the required momentum c_μ. The quadratic symbols represent the case $F^+ = 0.8$, $\Delta = 50\%$ with different flow rates or different p_V, respectively. The triangles denote points of constant c_μ but with varying frequencies and irrespective of whether the momentum was made by longer duty cycles or by higher exit velocities. Unlike for the suction-side actuation, for which the best results were achieved with $c_\mu \approx 0.023\%$, an increase of the injected momentum increases the effectiveness up to a certain threshold. But the maximum normal force $c_{np,\max}$ is not reached with the maximum momentum; there is a weak optimum around $c_\mu \approx 0.25\%$. Again, unlike for the suction-side actuation, a further increase of c_μ is not destructive but also not

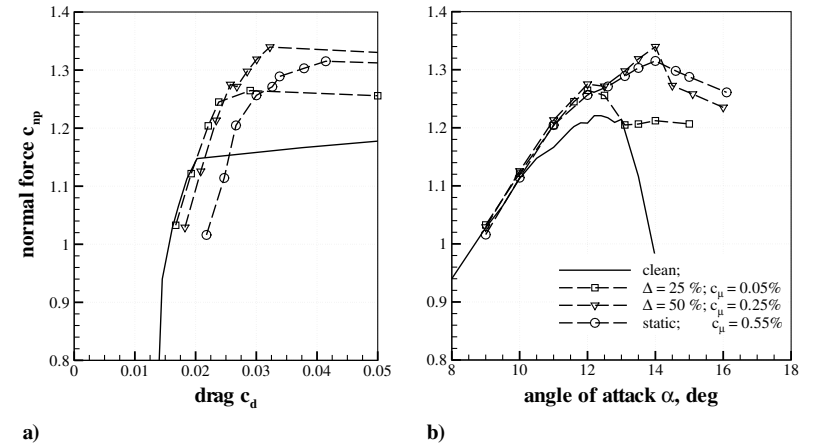

Fig. 10 Variation of duty cycle Δ with $F^+ = 1.44$ and $p_V = 3.0$ bar for the pressure-side configuration: a) drag polar, and b) normal force coefficient over AOA.

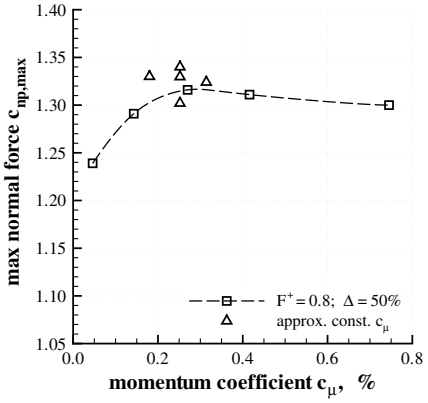

Fig. 11 Maximum normal force $c_{np,\max}$ with respect to momentum coefficient c_μ for constant frequency and duty cycle and for oblique cases with approximately the same c_μ.

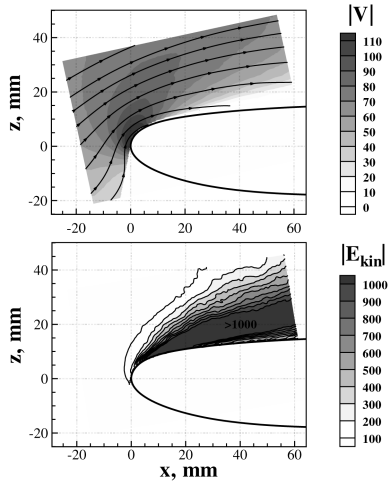

Fig. 12 Velocity magnitude $|V|$ (m/s), streamlines (upper panel), and turbulent kinetic energy E_{kin} (m^2/s^2) for $\alpha = 15$ deg; $F^+ = 1.44$, $\Delta = 50\%$, and $p_V = 3.0$ bar ($c_\mu = 0.25\%$).

beneficial. Nevertheless, the maximum normal force is influenced by the other parameters as well, as the different configurations with roughly the same c_μ differ in $c_{np,\max}$. The highest normal force was measured with $F^+ = 1.44$ and $\Delta = 50\%$ while $c_\mu \approx 0.25\%$. The duty cycle does have an influence, but in contrast to the suction-side actuation it is not vital for the pressure-side actuation.

To reveal the same information as for the suction-side actuation, PIV measurements were performed using the same setup. In Fig. 12, the velocity magnitude and the turbulent kinetic energy are plotted for $\alpha = 15$ deg with active control with $F^+ = 1.44$, $\Delta = 50\%$, and $p_V = 3.0$ bar, which gave the maximal normal force. The streamlines indicate that the flow is fully attached at the leading edge. Note the very high level of turbulent kinetic energy, which is much higher than it had been in the stalled cases with the suction-side actuation (Fig. 8).

Somewhat abnormal is the fact that the streamlines tend to run into the airfoil surface. This indicates that only the temporal mean of the flow appears attached; the individual recordings (not shown) highlight that the flow is highly unsteady with large scale vortices present. Phase locking the PIV system to the actuator's process did not provide further insight, which in turn implies that the unsteadiness of the separation is not directly linked to the actuator's periodicity.

By positioning the actuator on the lower side, not only was the upstream distance to the separation line varied, but so were the conditions for the actuator. Boundary-layer parameters cannot simply be measured, therefore a comparison is made on the basis of calculations with the XFOIL code. The left part of Fig. 13 displays the measured and calculated pressure distributions for the airfoil (calculated to fit the measured c_{np}). Because the pressure distributions fit very well, it can be expected that the edge velocity u_e and the momentum thickness Θ from the XFOIL calculations are realistic.

On the right side of Fig. 13, the arc length along the airfoil's contour is plotted at the axis of abscissae, with the stagnation point at the origin. The positions of the actuators are indicated, too. As can be seen, the suction-side actuator is faced with $\Theta = 0.033$ mm and $u_e = 138$ m/s, whereas for the pressure-side actuator these values are $\Theta = 0.012$ mm and $u_e = 52$ m/s. The change of the momentum thickness between the configurations does not seem to be very vital, as both are much smaller than the actuator's dimensions. But the actuation is now at a position where the edge velocity is relatively low, before acceleration, hence for a given (and usually limited) u_j the local velocity ratio based on edge velocity λ_e is increased substantially. For the generation process of longitudinal vortices, λ_e is a very influential factor; here it is raised significantly without raising c_μ. The high streamline curvature around the nose as well as the pressure gradients do not appear to be a major problem for the vortices.

VI. Conclusions

Two different actuation configurations have been tested on an airfoil to benchmark their ability to prevent or influence a turbulent leading-edge stall. For these configurations, a number of operational

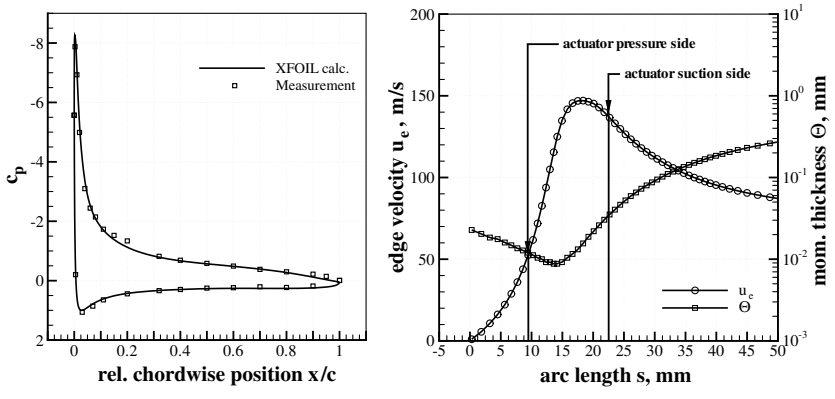

Fig. 13 Boundary-layer properties around the points of actuation: a) measured and calculated pressure distributions (measurement: $\alpha = 12.0$ deg; XFOIL calculated to same $c_{np} = 1.2$), and b) edge velocity u_e and momentum thickness Θ taken from XFOIL.

parameters, namely, frequency, duty cycle, and actuation amplitude, were varied to study their influence on the process.

If the actuation was positioned at $x/c = 1.0\%$ on the suction side, all sets of operational parameters had a similar effect, where the stall was not prevented, but the normal force coefficient c_{np} was raised distinctly in the poststall. The most successful cases were $f = 75$ Hz at $\Delta = 12\%$ or $\Delta = 25\%$ duty cycle, where $c_{np,\max}$ was raised by $\Delta c_{np,\max} \approx 0.1$ or 8%, respectively. The excitation frequency showed a small influence on the stall behavior; the duty cycle Δ, on the other hand, turned out to have major influence. The experiments with the pressure-side actuation are a poststall flow control scenario or a control of separated flow, but not a delay of separation.

The position of the actuation was moved upstream to a position $x/c = 1.0\%$ on the airfoil pressure side in between the leading edge and the stagnation point. This kind of setup resulted in a successful vortex generator jet kind of separation control, in which the stall was delayed and an almost continuous lift curve resulted. The maximum AOA was increased by $\Delta\alpha_{\max} \approx 2.5$ deg, the maximum normal force by $\Delta c_{np} \approx 0.15$. With active control, the drag increased only little, making this configuration quite interesting for practical applications. PIV measurements showed that the pressure-side actuation leads to very unsteady flow over the airfoil, which is only attached in the temporal mean. As a drawback, the amplitude required to delay separation is an order of magnitude larger than the amplitude required to control the separated flow with the suction-side setup

It was discussed that moving the position of actuation changed the boundary conditions of the actuators in two ways. First, there is a longer distance between the actuators and the separation line, and therefore the blocked area of the vortex generator jets is shifted away from the line of separation. Second, the edge velocity changes drastically with different positions near the suction peak, hence the local velocity ratio λ_e can be increased significantly by simply using a different position for actuation.

To increase the efficiency, the optimal upstream position has to be found in the first instance, although the variation of this parameter is a challenging problem. It would be interesting to find evidence if the distance to separation or the virtually increased λ_e is the key factor; for practical blowing systems, one is limited to the speed of sound as the exit velocity. In the pressure-side setup a small amplitude is ineffective, and in the suction-side setup the velocity ratio is limited to $\lambda_e \approx 2.6$ due to this limitation of u_j. However, vortex generator jets near the pressure minimum are obviously less effective in preventing separation than those that are closer to the stagnation point with a considerably lower u_e.

To carefully optimize the whole system, the development of longitudinal vortices in strong favorable and adverse pressure gradients must be studied.

Acknowledgment

The project is part of Lufo III Innovative Hochauftriebskonfigurationen (IHK) of the Federal Ministry of Economics and Technology (BMWi). It is being dealt with as a participant of the joint research project Dynamische 3D Strömungskontrolle.

References

[1] Schlichting, H., *Boundary-Layer Theory*, 6th ed., McGraw–Hill, New York, 1968, pp. 644–648, Chap. 22.

[2] Englar, R. J., "Circulation Control for High Lift and Drag Generation on STOL Aircraft," *Journal of Aircraft*, Vol. 12, No. 5, 1975, pp. 457–463.

[3] Seifert, A., Bachar, T., Wygnanski, I., Koss, D., and Shepshelovich, M., "Oscillatory Blowing: A Tool to Delay Boundary-Layer Separation," *AIAA Journal*, Vol. 31, No. 11, 1993, pp. 2052–2060.

[4] Seifert, A., and Pack, L, G., "Oscillatory Excitation of Unsteady Compressible Flows over Airfoils at Flight Reynolds Numbers," AIAA Paper 99-0925, 1999.

[5] Amitay, M., and Glezer, A., "Role of Actuation Frequency in Controlled Flow Reattachment over a Stalled Airfoil," *AIAA Journal*, Vol. 40, No. 2, 2002, pp. 209–216.

[6] Nishri, B., and Wygnanski, I., "Effects of Periodic Excitation on Turbulent Flow Separation from a Flap," *AIAA Journal*, Vol. 36, No. 4, 1998, pp. 547–556.

[7] Seifert, A., Eliahu, S., Greenblatt, D., and Wygnanski, I., "Use of Piezoelectric Actuators for Airfoil Separation Control," *AIAA Journal*, Vol. 36, No. 8, 1998, pp. 1535–1537.

[8] Smith, D. R., "Interaction of a Synthetic Jet with a Crossflow Boundary Layer," *AIAA Journal*, Vol. 40, No. 11, 2002, pp. 2277–2288.

[9] Schatz, M., Thiele, F., Petz, R., and Nitsche, W., "Separation Control by Periodic Excitation and Its Application to a High Lift Configuration," AIAA Paper 2004-2507, 2004.

[10] Pauley, W. R., and Eaton, J. K., "Experimental Study of the Development of Longitudinal Vortex Pairs Embedded in a Turbulent Boundary Layer," *AIAA Journal*, Vol. 26, No. 7, 1988, pp. 816–823.

[11] Fiedler, H. E., and Fernholz, H.-H., *On Management and Control of Turbulent Shear Flows*, Progress in Aerospace Science, Vol. 27, Pergamon, Oxford, England, U.K./New York, 1991, pp. 305–387.

[12] Godard, G., and Stanislas, M., "Control of a Decelerating Boundary Layer. Part 1: Optimization of Passive Vortex Generators," *Aerospace Science and Technology*, Vol. 10, No. 3, 2006, pp. 181–191. doi:10.1016/j.ast.2005.11.007

[13] McManus, K. R., Joshi, P. B., Legner, H. H., and Davis, S. J., *Active Control of Aerodynamic Stall Using Pulsed Jet Actuators*, AIAA Paper 95-2187, 1995.

[14] Johnston, J., Nishi, M., "Vortex Generator Jets: Means for Flow Separation Control," *AIAA Journal*, Vol. 28, No. 6, 1990, pp. 989–994.

[15] Suzuki, T., Nagata, M., Shizawa, T., and Honami, S., "Optimal Injection Condition of a Single Pulsed Vortex Generator Jet to Promote the Cross-Stream Mixing," *Experimental Thermal and Fluid Science*, Vol. 17, No. 1, 1998, pp. 139–146. doi:10.1016/S0894-1777(97)10059-0

[16] Zhang, X., and Collins, M. W., "Measurements of a Longitudinal Vortex Generated by a Rectangular Jet in a Turbulent Boundary Layer," *Physics of Fluids*, Vol. 9, No. 6, 1997, pp. 1665–1673.

[17] Godard, G., and Stanislas, M., "Control of a Decelerating Boundary Layer. Part 2: Optimization of Slotted Jets Vortex Generators," *Aerospace Science and Technology*, Vol. 10, No. 5, 2006, pp. 394–400. doi:10.1016/j.ast.2005.11.006

[18] Tilmann, C. P., Langan, K. J., Betterton, J. G., and Wilson, M. J., "Characterization of Pulsed Vortex Generator Jets for Active Flow Control," Air Force Research Laboratory AFRL-VA-WP-TP-2003-336, Wright-Patterson Air Force Base, 2003.

[19] Scholz, P., Ortmanns, J., Kähler, C. J., and Radespiel, R., "Influencing the Mixing Process in a Turbulent Boundary Layer by Pulsed Jet Actuators," "*New Results in Numerical and Experimental Fluid Mechanics V*", Notes on Numerical Fluid Mechanics and Multidisciplinary Design, Vol. 92, Springer–Verlag, pp. 265–272, 2006.

[20] Fasel, H. F., Gross, A., and Postl, D., "Numerical Simulation of Active Flow Control for Low Pressure Turbine Blades," NATO Research and Technology Organisation RTO-MP-AVT-111, 2004.

[21] Wu, J. Z., Lu, X. Y., Denny, A. G., Fan, M., and Wu, J. M., "Post-Stall Flow Control on an Airfoil by Local Unsteady Forcing," *Journal of Fluid Mechanics*, Vol. 371, Sept. 1998, pp. 21–58. doi:10.1017/S0022112098002055

[22] Lachmann, G. V., *Boundary Layer and Flow Control: Its Principles and Application*, Vol. 1, Pergamon, London, 1961.

[23] Barlow, J. B., Rae W. H. Jr., and Pope, A., *Low-Speed Wind Tunnel Testing*, Wiley–Interscience, New York, 1999.

[24] Drela, M., and Youngren, H., *XFOIL 6.94 User Guide*, Massachusetts Inst. of Technology, Dept. of Aeronautics and Astronautics, Cambridge, MA, 2001.

[25] Drela, M., *A User's Guide to MSES 2.95*, Massachusetts Inst. of Technology, Computational Aerospace Sciences Laboratory, Cambridge, MA, 1996.

[26] Ortmanns, J., and Kähler, C. J., "Investigation of Pulsed Actuators for Active Flow Control Using Phase Locked Stereoscopic Particle Image Velocimetry," *12th International Symposium for Application of Laser Techniques to Fluid Mechanics*, June 2004.

[27] Scholz, P., Ortmanns, J., Kähler, C. J., and Radespiel, R., "Performance Optimization of Jet Actuator Arrays for Active Flow Control," *CEAS/KATnet-Conference on "Key Aerodynamic Technologies"*, June 2005.

[28] Kähler, C. J., Scholz, P., Ortmanns, J., and Radespiel, R., "Towards Active Control of Leading Edge Stall by Means of Pneumatic Actuators," *Active Flow Control*, Notes on Numerical Fluid Mechanics

and Multidisciplinary Design, Vol. 95, Springer–Verlag, 2007, pp. 152–172.
[29] Jones, B. M., "The Measurement of Profile Drag by the Pitot Traverse Method," Aeronautical Research Council RM 1688, 1936.
[30] Stanislas, M., Okamoto, K., Kähler, C. J., and Westerweel, J., "Main Results of the Second International PIV Challenge," *Experiments in Fluids*, Vol. 39, No. 2, 2005, pp. 170–191. doi:10.1007/s00348-005-0951-2
[31] Winkelmann, A. E., and Barlow, J. B., "Flowfield Model for a Rectangular Planform Wing Beyond Stall," *AIAA Journal*, Vol. 18, No. 8, 1980, pp. 1006–1008.
[32] Hites, M., Nagib, H., Bachar, T., and Wygnanski, I., *Enhanced Performance of Airfoils at Moderate Mach Numbers Using Zero Mass Flux Pulsed Blowing*, AIAA Paper 2001-0734, 2001.

N. Clemens
Associate Editor